Design Compact Dual Band EMSIW MIMO Antenna with Improved Higher-Order Mode Radiation Pattern

Nidhi Yadav[1$*], Rajendra Prasad Yadav[2$], M. M. Sharma[3$]
[$]*Department of ECE, Malviya National Institute of Technology,* Jaipur, India-302017
*Corresponding Author Mobile Number- +91-9636516110
[1]2021rec9502@mnit.ac.in, [2]rpyadav.ece@mnit.ac.in, [3]mms.ece@mnit.ac.in

1. Present address: *Department of Electronics and Communication Engineering, Malviya National Institute of Technology, JLN Marg* Jaipur, India-302017

***Abstract*— In this paper, a compact dual-band eight-mode substrate-integrated waveguide (EMSIW) MIMO (Multiple-Input Multiple-Output) antenna is presented for S and C band applications. By utilizing the EMSIW approach, the electrical size of the antenna is reduced to 1/8th of a conventional square SIW cavity resonator. The eight-mode configuration preserves the dominant mode at the same frequency, while significantly reducing the antenna size. The dominant mode resonates at 2.5 GHz, and a higher-order mode operates at 5.8 GHz by incorporating a slot in the design. To improve the radiation pattern at 5.8 GHz, the surface current nulls near the center of the EMSIW patch are reshaped, enhancing broadside radiation. The 2x2 MIMO antenna is designed to minimize mutual coupling by maintaining specific electric and magnetic wall configurations, ensuring minimal electric field interaction between the antenna ports. Fabricated on a low-cost FR4 substrate, the proposed MIMO antenna demonstrates excellent agreement between simulated and measured results. This compact design is a promising solution for satellite S-band and C-band applications, offering enhanced higher-order mode radiation performance and minimal mutual coupling.**

***Index Terms*—** MIMO Antenna, SIW, EMSIW, S band, c band, higher order mode.

I. INTRODUCTION

The rapid development of wireless communication systems, particularly in the S and C bands, demands compact and efficient antennas with multi-band operation and minimal interference between antenna elements. The MIMO antenna systems play a critical role in meeting these requirements, as they enhance data rates and system capacity by exploiting spatial diversity and multiplexing [1-2]. However, achieving compactness in MIMO designs while maintaining performance, especially at higher frequencies, remains a significant challenge. One approach to address this issue is through the use of substrate-integrated waveguide (SIW) technology, which offers high performance, low loss, and ease of integration, while ensuring reduced interference between ports in MIMO systems [3-5].

MIMO antennas designed for the S and C bands have a wide range of applications in modern wireless communication systems, where their ability to enhance data rates, improve capacity, and ensure signal reliability is highly valuable [6-8]. One of the primary applications is in **5G wireless networks**. In the **S band** (2–4 GHz), MIMO antennas support mid-band 5G frequencies, providing a balance between coverage and capacity. This makes them ideal for suburban and rural areas where long-range communication is essential [9]. On the other hand, the C band (4–8 GHz) is crucial for urban deployment, where high data rates and network efficiency are required to manage dense traffic [10]. The C-band spectrum in 5G networks offers a balance between coverage and capacity, enabling faster speeds without compromising range [11].

Another key application is in **satellite communications**, where both S and C bands are used for different purposes. The **S band** is employed in satellite systems for telemetry, tracking, and control (TT&C) operations, ensuring stable communication between ground stations and satellites [12-14]. MIMO technology in this band improves signal reliability and reduces interference through spatial multiplexing, which is essential for maintaining the quality of satellite links [15-17]. In the **C band**, MIMO antennas are extensively used in satellite-based communication systems, including broadcasting and internet services. The high resilience of C-band signals to rain fade makes them ideal for reliable, high-quality communication in tropical and subtropical regions [18-22].

Other notable applications include **radar systems** and **wireless backhaul networks**, where MIMO antennas in the S and C bands provide enhanced target detection, signal processing, and long-distance data transmission [23]. These bands are also used in **public safety communications**, ensuring robust and reliable links in emergency and disaster management scenarios. The ability of MIMO technology to minimize interference and optimize bandwidth utilization makes it essential in these critical applications [24].

Substrate-Integrated Waveguide (SIW) technology is widely used for high-frequency applications due to its ability to confine electromagnetic waves between two metalized via arrays, providing characteristics similar to traditional waveguides but with the advantages of planar structures. However, conventional SIW cavity resonators are often limited in size, posing challenges for compact designs [8-12]. To overcome this, a miniaturized SIW configuration known as the Eight-Mode Substrate-Integrated Waveguide (EMSIW) has been introduced. EMSIW reduces the electrical size of the resonator to 1/8th of that of a conventional SIW cavity, while maintaining the desired electromagnetic properties [24-30]. The proposed EMSIW design allows for a significant size reduction without compromising performance.

A comprehensive literature survey reveals various dual-band MIMO antennas designed for S and C band applications, many of which rely on conventional SIW or microstrip technology. While these designs offer dual-band operation, they often suffer from larger sizes or higher mutual coupling, making them less ideal for compact wireless systems. The proposed EMSIW MIMO antenna stands out due to its novel use of miniaturized SIW technology and innovative design strategies to enhance radiation patterns while maintaining low mutual coupling.

The proposed compact dual-band eight-mode EMSIW MIMO antenna introduces several novel design aspects targeting S- and C-band applications. This work advances the concept by reducing the antenna's electrical size to one-eighth of a conventional square SIW cavity resonator without compromising the dominant mode operation at 2.5 GHz. A higher-order mode at 5.8 GHz is excited through strategic slot incorporation, enabling efficient dual-band functionality. Additionally, to enhance broadside radiation at 5.8 GHz, the current distribution is modified by reshaping nulls near the center of the EMSIW patch. The proposed 2×2 MIMO configuration further improves performance by employing optimized electric and magnetic wall boundaries, which effectively reduce mutual coupling and electric field interaction between antenna elements. This integration of slot-assisted higher-order mode excitation, radiation pattern enhancement, and improved MIMO isolation within a miniaturized EMSIW framework represents a significant advancement over existing designs and establishes the antenna as a strong candidate for compact satellite communication systems in the S- and C-band.

II. DESIGN OF DUAL BAND EMSIW ANTENNA

A. Proposed Antenna Geometry

Figure 1 illustrates the schematic design of a compact dual-band Eight-Mode Substrate-Integrated Waveguide (EMSIW) antenna and its 2x2 MIMO configuration. Figure 1(a) shows the layout of a single EMSIW antenna element. The EMSIW approach enables significant miniaturization compared to conventional SIW designs by reducing the electrical size to 1/8th of that of a typical SIW cavity. The triangular slot and circular resonators (marked by $\mathbf{r_1}$, $\mathbf{r_2}$, and $\mathbf{r_3}$) are key design features that tune the antenna's higher-order mode resonance, specifically at 5.8 GHz. The electrical field and surface current distribution are tailored by these elements to enhance the broadside radiation pattern.

The dotted circular pattern near the bottom of the antenna represents the array of metalized vias, which confine the electromagnetic fields within the waveguide, ensuring low loss and proper wave propagation. Figure 1(b) shows the 2x2 MIMO antenna configuration created by replicating the single EMSIW antenna four times in a symmetrical arrangement. The overall size of the MIMO structure, which is compact, with an area of 50 × 50 × 2.4 mm^3, making it suitable for 5G applications. The physical parameters of proposed antenna represented in Table-I. The MIMO configuration is designed to minimize mutual coupling between the individual antenna elements, as the electric and magnetic walls within the EMSIW structure help to reduce interference between ports.

B. **Modal Analysis of Square SIW Antenna**

Figures 2 and 3 provide a detailed modal analysis and electric field (E-field) distributions of various Substrate-Integrated Waveguide (SIW) resonators, highlighting their performance at fundamental and higher-order modes. In Figure 2, the comparison between different SIW configurations demonstrates how changes in the geometry lead to miniaturization and enhanced performance.

Starting with Figure 2(a), the standard square SIW resonator confines electromagnetic waves using metalized vias along the boundaries, creating electric and magnetic walls that define the waveguide's cavity. This configuration displays a uniform field distribution in the fundamental mode but has limited size reduction capabilities. To address this, Figure 2(b) shows the Full Mode SIW (FMSIW), which reduces the antenna's electrical size by folding the structure, effectively concentrating the energy towards the boundaries. This modification enables compactness while maintaining effective electromagnetic wave propagation. Further miniaturization is demonstrated in Figure 2(c) with the Quarter-Mode SIW (QMSIW) resonator, which reduces the original square cavity to one-quarter of its size by introducing both electric and magnetic walls in a strategic layout. The field distribution is no longer symmetric, as energy is confined to a smaller region, allowing for a significant reduction in size without altering the resonance frequency. Finally, Figure 2(d) presents the Eight-Mode SIW (EMSIW) resonator, which achieves even more substantial miniaturization by reducing the size to 1/8th of the conventional SIW cavity. The triangular and slot modifications in this design reshape the field distribution, enabling the resonator to operate at dual bands while maintaining a compact form factor, crucial for applications such as MIMO antennas.

Figure 3 complements this modal analysis by illustrating the E-field distributions of the square SIW resonator across different operating modes. In Figure 3(a), the E-field at the fundamental mode (2.5 GHz) exhibits a symmetric distribution across the square cavity, with the strongest field intensity at the center, which is typical for low-frequency operation. At higher frequencies, as shown in Figures 3(b) and 3(c), the resonator excites two orthogonal higher-order modes at 4.5 GHz, where the E-field patterns become more complex with multiple nulls and peaks. These orthogonal modes are essential for dual-polarized or multi-band applications, as they provide different radiation characteristics at the same frequency. Finally, Figure 3(d) shows the E-field distribution at 5.8 GHz, where the resonator supports a higher-order mode with a highly localized and intricate field pattern. This mode is especially important in the EMSIW design as it enhances the broadside radiation, improving the antenna's performance at higher frequencies.

Together, these figures demonstrate the evolution from conventional square SIW resonators to more compact designs like FMSIW, QMSIW, and EMSIW, all of which achieve significant size reductions while maintaining or even improving performance in terms of dual-band operation and radiation characteristics. The modal analysis and field distribution provide valuable insights into how these SIW configurations manipulate the electromagnetic fields to achieve miniaturization and performance optimization, making them suitable for modern wireless communication systems, particularly in MIMO applications for S and C bands. The resonant frequency of the SIW resonator can be calculated using the equation given in [28]:

$$f_{mn0} = \frac{c}{2\sqrt{\varepsilon_r}} \sqrt{\left(\frac{m}{L_{eff}}\right)^2 + \left(\frac{n}{W_{eff}}\right)^2} \qquad \text{Eq. (1)}$$

where c is the speed of light in a vacuum, ε_r is the relative permittivity of the substrate, and m and n are the mode numbers. The effective width and length of the SIW cavity L_{eff}, and W_{eff} are given by the following equations:

$$L_{eff} = L_p - \frac{d^2}{0.95s} \qquad \text{Eq. (2)}$$

$$W_{eff} = W_p - \frac{d^2}{0.95s} \qquad \text{Eq. (3)}$$

Here, L_p and W_p represent the physical width and length of the SIW cavity, respectively. The parameters d and s denote the diameter of the vias and the spacing between them.

C. **Designing CRSL QMSIW Antenna**

Figure 4 illustrates the evolution of the SIW antenna, focusing on miniaturization techniques and performance improvements. The explanation begins with Fig. 3(a), which shows a conventional QMSIW antenna. This configuration divides the original SIW cavity into a quarter, with two sides having electric walls (EW) and the other two sides having magnetic walls (MW). The magnetic walls are responsible for the radiation of the fundamental mode, while a non-contact coaxial feed excites the mode within the cavity. This design significantly reduces the antenna's size while maintaining the same resonant frequency, offering a compact solution for wireless communication applications.

Moreover, the current distribution is more intense along the magnetic walls, as depicted in Fig. 5(a), which highlights the contrast in surface current density between the magnetic and electric walls. This behavior is essential for understanding how the quarter-mode operation efficiently uses space while preserving radiation performance.

Fig. 5 (b) provides a parametric study of the antenna's S11 plot. This plot is crucial for examining the antenna's impedance matching, which can be adjusted by strategically placing the feed. The antenna's impedance and resonant frequency are greatly influenced by the feed position; designers can ensure that the antenna obtains a good match (low S11 value) at the intended operating frequency by modifying the feed location. This parametric analysis demonstrates of the QMSIW design, as the feed location can be modified to optimize the antenna's performance.

Fig. 5 (c) displays the far-field radiation pattern of the QMSIW antenna operating at a frequency of 2.5 GHz for two different angle planes, phi = 0° and phi = 90°. In both cases, the antenna exhibits broadside radiation, meaning that the majority of the energy it emits is oriented perpendicular to the plane of the antenna. This broadside radiation is a characteristic of the antenna's fundamental mode, where the fields are symmetrically distributed across the antenna's surface, allowing for efficient radiation in the desired direction. At this fundamental mode of operation, the antenna achieves a gain of 3.8 dBi(theta=0°), which indicates a moderately focused radiation pattern.

Fig. 3(b) introduces the Eight-Mode Substrate-Integrated Waveguide (EMSIW) antenna, which further reduces the size by using a triangular cavity shape. The triangular design not only decreases the electrical size but also allows for efficient field confinement due to the strategic placement of the magnetic and electric walls. The parametric study in Fig. 6(a) illustrates the impact of varying the substrate height (h) on the bandwidth performance of the EMSIW antenna. Increasing the substrate height from 0.8 mm to 3.2 mm leads to a noticeable shift in the resonant frequency and broader bandwidth, but at the cost of higher surface wave losses and increased mutual coupling. Therefore, a substrate height of 2.4 mm is considered an optimal choice, offering a trade-off between performance and structural efficiency. The EMSIW antenna is perfect for applications requiring compact antennas since it supports dual band at 2.5 GHz and 5.8 GHz while keeping compact dimensions. The corresponding S11 plots shown in Fig.6(b).

The radiation patterns of the dual-band EMSIW antenna are shown in Fig. 6(c) and Fig. 6(d) for its two operating frequencies: 2.5 GHz and 5.8 GHz, respectively. At 2.5 GHz, the antenna operates in its fundamental mode, and the radiation patterns are plotted for two angular planes, phi = 0° and phi = 90°. In both planes, the antenna demonstrates broadside radiation. At this frequency, the antenna achieves a gain of 2.5 dBi at theta = 0°, indicating that the antenna effectively radiates energy in the desired direction with moderate focus and efficiency.

At the higher frequency of 5.8 GHz, the antenna operates in a higher-order mode, and the radiation pattern undergoes a significant change. As shown in Fig. 6(d), the radiation pattern becomes conical for both phi = 0° and phi = 90° planes. This conical radiation indicates that the energy is no longer focused in the broadside direction but instead radiates at an angle off the main axis, creating a doughnut-shaped pattern. The antenna shows a gain of -0.5 dBi at theta = 0° at this higher frequency, which is less than the gain at 2.5 GHz.

The reduction in gain at 5.8 GHz is attributed to surface current nulls or out-of-phase current distributions near the center of the antenna, as shown in Fig. 7. These surface current nulls result in destructive interference, reducing the overall radiation efficiency in the broadside direction. The higher-order mode creates these current distributions, leading to a more complex radiation pattern and a decrease in gain at the higher frequency. Despite this, the antenna's dual-band capability offers flexibility for applications that require both broadside radiation at lower frequencies and more specialized radiation patterns at higher frequencies.

Finally, Fig. 3(c) presents the slot-loaded EMSIW antenna, which incorporates circular slots into the triangular EMSIW cavity. These slots modify the surface current distribution, enabling better control of the resonant frequencies and improving the radiation pattern in broadside direction, especially at higher-order modes. This design allows for dual-band operation, with one mode operating at a lower frequency and the other at a higher frequency. The slot-loaded EMSIW antenna is optimized for enhanced performance while remaining compact, making it well-suited for dual-band applications like 5G and other modern wireless systems.

Fig. 8(a) and Fig. 8(b) present a parametric study of the r2 and l2 parameters of the slotted EMSIW antenna. By varying these parameters, the antenna's operating frequency and surface current distribution are significantly affected, allowing the antenna to resonate at both 2.5 GHz and 5.8 GHz with enhanced radiation patterns and improved gain in the broadside direction. The careful tuning of these parameters ensures that the antenna operates efficiently at these frequencies while optimizing its radiation characteristics.

The slotted EMSIW antenna's surface current distribution at 2.5 GHz and 5.8 GHz is displayed in Fig. 9. The antenna is functioning in its fundamental mode at 2.5 GHz, with a uniform current distribution throughout its surface. However, at 5.8 GHz, surface current nulls are observed near the center of the antenna. These current nulls are a result of out-of-phase current distributions that occur at the higher frequency, affecting the radiation performance and shaping the far-field patterns.

For the two operating frequencies of 2.5 GHz and 5.8 GHz, respectively, the corresponding far-field radiation patterns are displayed in Figures 10(a) and 10(b). The radiation patterns are presented for the angular plane’s phi = 0° and phi = 90° at 2.5 GHz, when the antenna is operating in its fundamental mode and radiating primarily in the broadside direction. The maximum radiation is directed perpendicular to the antenna surface, achieving a directive gain of 2.6 dBi at theta = 0°, signifying that the antenna radiates effectively in the desired direction with moderate efficiency and focus.

The radiation pattern changes as a result of the antenna entering a higher-order mode at the higher frequency of 5.8 GHz. The far-field radiation in the broadside direction shows an improved directive gain of around 5.2 dBi for both phi = 0° and phi = 90° planes, indicating a more focused and efficient radiation in this higher-order mode compared to the fundamental mode. This significant improvement in directive gain at 5.8 GHz is due to the optimization of the slot dimensions (r2 and l2) and the management of surface currents, which help reduce the negative effects of current nulls near the center of the antenna, thereby enhancing the radiation performance in the higher frequency band.

III. PERFORMANCE ANALYSIS OF SLOTTED EMSIW ANTENNA

A. Performance of Mutual Coupling for MIMO Antenna

Fig. 11 illustrates the configuration of antenna elements in a 2×2 MIMO system and focuses on how the orientation of electric walls (EW) and magnetic walls (MW) influences the mutual coupling between these elements. Mutual coupling refers to the interaction between antennas that can degrade their performance by reducing isolation. Minimizing this coupling is critical in MIMO systems, where high isolation improves channel capacity and overall system performance.

In Fig. 11(a), the antennas are positioned so that the electric walls of one antenna face the magnetic walls of the adjacent antenna. This arrangement leverages the different characteristics of electric and magnetic fields. The electric fields are primarily confined within the substrate near the electric walls, whereas the magnetic fields are dominant near the magnetic walls. By positioning the electric and magnetic walls to face each other, the interaction between antennas is reduced, but there is still mutual coupling at the magnetic walls. This is undesirable in MIMO systems as high mutual coupling can degrade isolation and reduce performance. The scattering parameters (S-parameters) corresponding to this configuration are shown in Fig. 12.

At a lower frequency of 2.5 GHz, the existence of magnetic walls at the operating frequency range near 2.4 GHz causes mutual coupling to be more noticeable at about -10 dB. However, at 5.8 GHz, the coupling is much lower, as the electric walls help to improve isolation between antenna elements at higher frequencies.

The electric field distribution for this configuration, shown in Fig. 13, highlights how the electric and magnetic fields interact at 2.5 GHz and 5.8 GHz.

In Fig. 11(b), the antennas are positioned with their magnetic walls facing each other. Since the magnetic walls in the EMSIW (Enhanced Mode Substrate-Integrated Waveguide) technology are responsible for supporting the antenna's radiation by directing the magnetic field flow, this configuration leads to stronger interactions between antenna elements, increasing mutual coupling.

However, by increasing the distance between the antennas and optimizing design parameters, the effects of mutual coupling can be mitigated as shown in Fig.14 for mutual coupling with l2 parameters. The scattering parameters for this configuration are shown in Fig. 15. At 2.5 GHz, the coupling is significantly reduced to -26 dB, and at 5.8 GHz, the coupling is also low, around -25.5 dB. The improved isolation is a result of careful positioning and design of the magnetic walls. The corresponding electric field distributions for this configuration at 2.5 GHz and 5.8 GHz are shown in Fig. 16, illustrating how the fields interact with each other at these frequencies.

This figure highlights the importance of the physical arrangement of antenna elements in MIMO systems. The orientation of electric and magnetic walls is crucial in controlling the extent of mutual coupling, which directly affects the isolation and overall system performance. For MIMO applications, achieving high isolation between antenna elements is key to ensuring multiple independent signal paths, which is essential for high data rates, better signal quality, and improved reliability in wireless communication systems

Fig.17(a) shows the top-view arrangement of the eight antenna elements in a 4×4 configuration, designed symmetrically to enhance spatial diversity and reduce mutual coupling. Fig.17(b) presents the S11-parameters (S11 to S88) of all ports, indicating good impedance matching across the operating bands with return loss values below –10 dB, ensuring efficient radiation. Fig. 17(c) displays the mutual coupling parameters (S21 to S81), where isolation levels are observed to be better than –15 dB, with some values reaching below –30 dB, confirming effective inter-element isolation.

B. Diversity Performance of proposed EMSIW MIMO antenna.

In addition to isolation and radiation patterns, a critical factor in evaluating the performance of MIMO antennas is their diversity capabilities. Diversity plays a crucial role in enhancing signal reliability and data throughput, especially in multipath environments where signals can reflect off various surfaces before reaching the receiver. Two key metrics used to assess diversity performance are the Envelope Correlation Coefficient (ECC) and Diversity Gain (DG).

The Envelope Correlation Coefficient (ECC) quantifies the degree of correlation between the signals that various antenna elements receive. Because it indicates that the signals are less coupled and that the antenna elements are capturing distinct multipath components of the signal, a lower ECC value is desirable. This improves the system's overall diversity performance by allowing it to process independent signal paths more effectively. Essentially, lower ECC values lead to better spatial diversity, enabling the system to distinguish between multiple signal paths, which can enhance communication reliability and data rates. ECC can be calculated using the complex radiation patterns of the antennas, and when the far-field radiation characteristics are known, a mathematical formula can be applied to estimate the ECC between two antenna elements. By designing a MIMO antenna system with low ECC and high diversity gain, the antenna can perform optimally in environments with significant signal reflections, such as urban or indoor settings, leading to more stable communications and higher throughput [10-14].

$$\boldsymbol{\rho_{12}} = \frac{\left|\iint_0^{4\pi}[\vec{F}_1(\theta,\emptyset) X \vec{F}_2(\theta,\emptyset) d\Omega]\right|^2}{\iint_0^{4\pi}\left|\vec{F}_1(\theta,\emptyset)\right|^2 d\Omega \iint_0^{4\pi}\left|\vec{F}_2(\theta,\emptyset)\right|^2 d\Omega} \qquad \text{Eq. (4)}$$

Where, $\boldsymbol{\rho_{12}}$ represent the ECC. $\vec{F}_1(\theta, \emptyset)$ and $\vec{F}_2(\theta, \emptyset)$ are the far-field radiation patterns for port-1 and port-2 of this MIMO antenna.

Alternatively, the ECC can be derived from the S-parameters [4-8]:

$$\text{ECC}=\frac{|S_{11}*S_{12}+S_{21}*S_{22}|^2}{(1-|S_{11}|^2-|S_{21}|^2)(1-|S_{22}|^2-|S_{12}|^2)} \qquad \text{Eq. (5)}$$

The antenna's reflection and transmission coefficients are S11/S22 and S21/S12, respectively. Fig. 18(a) displays ECC plots derived from simulated and measured data, demonstrating <0.001 at 2.5GHz and 5.8 GHz.

Diversity Gain (DG) refers to the improvement in signal quality and reliability achieved by using multiple antennas in a MIMO system. It shows how effectively the system mitigates the impacts of interference and signal fading to improve the Signal-to-Noise Ratio (SNR). To reduce signal degradation brought on by multipath propagation, DG essentially calculates the advantage of receiving numerous versions of the transmitted signal along various pathways.

A higher diversity gain indicates that the system can maintain a stronger, more stable signal even in environments prone to significant signal fading, such as urban areas with numerous obstacles or indoor settings. This improvement in SNR leads to more reliable communication with fewer errors and increased

data throughput. As the diversity gain increases, the system becomes more resilient to the challenges of fading, improving both the consistency and the overall performance of the communication link.
For a two-antenna system, the Diversity Gain (DG) can typically be approximated by specific mathematical expressions based on the statistical properties of the received signals, allowing engineers to evaluate the effectiveness of the MIMO system in leveraging spatial diversity. By maximizing DG alongside minimizing ECC, MIMO systems can significantly boost performance in multipath environments

$$DG \approx 10\sqrt{1-(ECC)^2} \quad \text{Eq. (6)}$$

where the ECC is zero (i.e., the signals are completely uncorrelated), the maximum diversity gain is 10 dB. Fig.18(b) illustrates the diversity gain derived from both simulated and measured data. The 3D radiation pattern performance at 2.5GHz and 5.8GHz is displayed in Figures 18(c) and 18(d), respectively.

III. HARDWARE FABRICATION AND MEASUREMENT

The 2×2 MIMO antenna was fabricated using a 50×50 mm² FR4 substrate with a thickness of 2.4 mm. The FR4 material was chosen due to its cost-effectiveness and well-suited dielectric properties for high-frequency applications. The fabrication process was carried out using a chemical etching method, ensuring precise implementation of the antenna design. The antenna design was integrated with 50-ohm SMA connectors to enable reliable coaxial feed connections, essential for accurate testing and performance evaluation.

The fabricated 2×2 MIMO antenna is shown in Figure 19(a) and Figure 19(b), which represent both front and back views, respectively. The antenna's intricate structure is seen in the front perspective. The back view illustrates the proper placement of the SMA connectors, ensuring minimal signal reflection and efficient power transmission. The antenna's performance was measured using a comprehensive test setup, as depicted in Figure 20(a). The setup includes a vector network analyzer (VNA) to evaluate parameters such as S-parameters, and mutual coupling. Additionally, the measurement process incorporated an anechoic chamber to measure radiation characteristics. The corresponding simulated and measured scattering parameters are compared in Fig. 20(b) and Fig. 20(c). The radiation performance at 2.4 GHz and 5.8 GHz is depicted in Fig. 20(d). The comparison with related published works is shown in Table II.

Table II provides a comparative analysis of the proposed antenna with recent state-of-the-art MIMO antenna designs. The proposed design stands out in several key aspects. First, it offers a highly compact form factor of $0.41\lambda_0 \times 0.41\lambda_0$, making it one of the smallest among the compared works—significantly smaller than designs in [4], [6], and [8], which have sizes exceeding $0.7\lambda_0$. Despite this miniaturization, the antenna supports dual-band operation at 2.5 GHz and 5.8 GHz, covering the S- and C-bands, whereas many prior designs operate over either a single band or higher frequencies not suitable for satellite or wireless communication applications. The gain achieved is 2.6 dBi at 2.5 GHz and 5.2 dBi at 5.8 GHz, which, although moderate, is comparable to or better than several larger antennas such as those in [4] and [5]. A major strength of the design lies in its exceptional port isolation exceeding 25.5 dB, which is significantly higher than the 20–22 dB range reported in most other works and even surpasses some advanced decoupling structures. Furthermore, the proposed antenna exhibits a very low Envelope Correlation Coefficient (ECC) of 0.001, indicating excellent diversity performance. These improvements are achieved through the integration of the eight-mode EMSIW cavity with an electric wall configuration, along with careful slot loading and surface current optimization. Collectively, the proposed antenna offers a compact, dual-band, and high-isolation solution ideal for modern MIMO applications.

IV. CONCLUSION

The proposed EMSIW-based antenna design successfully reduces the overall electrical size while preserving the dominant mode operation at 2.5 GHz. The introduction of a slot enables higher-order mode excitation at 5.8 GHz, resulting in enhanced broadside radiation performance through surface current redistribution. The 2×2 MIMO configuration effectively minimizes mutual coupling by utilizing artificial electric and magnetic wall structures, maintaining high isolation and low correlation between ports. Fabrication on a low-cost FR4 substrate confirms the practical feasibility of the design, with strong agreement observed between simulated and measured results. However, certain limitations must be acknowledged. The use of FR4 introduces dielectric losses, which may reduce radiation efficiency and gain, particularly at higher frequencies. Additionally, manufacturing tolerances could impact the repeatability and consistency of performance. Despite these challenges, the design remains a compact and high-performing candidate for S and C band MIMO applications. Future research will focus on improving gain through low-loss substrates, exploring reconfigurable or tunable structures, and extending the design to higher-order MIMO systems such as 4×4 and 8×8 configurations for advanced wireless communication scenarios.

REFERENCES

[1] Yuan Liping, Kai Sun, Sihao Liu and et al. "Wideband SIW half-mode/quarter-mode-fed microstrip patch complementary antennas with back radiation suppression." *IEEE Access* 9 (2021):48963-48970. https://doi.org/10.1109/AP-S/INC-USNC-URSI52054.2024.10686622.

[2] Shi Zhiwei, Guohui Li, Yulu Song, and et al. "Compact Quarter Mode and Eighth Mode Substrate Integrated Waveguide Bandpass Filters with Frequency-Dependent Coupling." *Progress In Electromagnetics Research Letters* 97 (2021). https://doi.org/10.2528/PIERL21012201.

[3] Wang Ni, and Xiaowen Xu. "A compact planar circularly polarized eighth-mode substrate integrated waveguide antenna." *International Journal of Microwave and Wireless Technologies* 10, no. 8 (2018): 956-967. https://doi.org/10.1017/S175907871800051X.

[4] Shariff BG Parveez, Tanweer Ali, Pallavi R. Mane, and et al. "Compact wideband two-element millimeter wave MIMO antenna with CMT based modified T-shaped decoupling structure for mobile applications with estimated link budget in urban scenario." *AEU-International Journal of Electronics and Communications* 177(2024):155209. https://doi.org/10.1016/j.aeue.2024.155209.

[5] Tran Huy-Hung, Tung The-Lam Nguyen, Hoai-Nam Ta, and et al. "A metasurface-based mimo antenna with compact, wideband, and high isolation characteristics for sub-6 ghz 5g applications." *IEEE Access* (2023). https://doi.org/10.1109/ACCESS.2023.3292303.

[6] Kim-Thi Phuong, Thang Nguyen Van, and Tung Bui Thanh. "A Self-Decoupling Technique for Isolation Enhancement in Closely-Spaced MIMO Patch Antennas." IEEE Antennas and Wireless Propagation Letters (2024). https://doi.org/10.1109/LAWP.2024.3367036.

[7] Hu Wei, Qiaosong Li, Hao Wu, and et al. "Dual-band antenna pair with high isolation using multiple orthogonal modes for 5G smartphones." IEEE Transactions on Antennas and Propagation 71, no. 2 (2023): 1949-1954. https://doi.org/10.1109/TAP.2022.3233458.

[8] Mahto Santosh Kumar, Ajit Kumar Singh, Rashmi Sinha, and et al. "High isolated four element MIMO antenna for ISM/LTE/5G (Sub-6GHz) applications." IEEE Access (2023). https://doi.org/10.1109/ACCESS.2023.3301185.

[9] Abubakar Hassan Sani, Zhiqin Zhao, Mehr E. Munir, and et al. "Enhanced smartphone connectivity: dual-band MIMO antenna with high isolation and low ECC." *Physica Scripta* 99, no. 6 (2024): 065524. https://doi.org/10.1088/1402-4896/ad4424.

[10] Deng Changjiang, Xiaowei Cao, Donghao Li, and et al. "Compact dual-band MIMO antenna with shared decoupling structure for 5G mobile terminals." IEEE Antennas and Wireless Propagation Letters 22, no. 6 (2023): 1281-1285. https://doi.org/10.1109/LAWP.2023.3240673.

[11] Wu Aiting, Yingxiang Tao, Pengquan Zhang, and et al. "A compact high-isolation four-element MIMO antenna with asymptote-shaped structure." Sensors 23, no. 5 (2023): 2484. https://doi.org/10.3390/s23052484.

[12] Agneessens Sam. "Coupled eighth-mode substrate integrated waveguide antenna: Small and wideband with high-body antenna isolation." IEEE Access 6 (2017): 1595-1602. https://doi.org/10.1109/ACCESS.2017.2779563.

[13] Agrawal Meha, and Trivesh Kumar. "A Semicircular Substrate Integrated Waveguide-Based Self-Diplexing Slot Antenna With Polarization Flexibility." IEEE Antennas and Wireless Propagation Letters 22, no. 7 (2023): 1518-1521. https://doi.org/10.1109/LAWP.2023.3249350.

[14] Chaturvedi Divya, and Arvind Kumar. "A QMSIW cavity-backed self-diplexing antenna with tunable resonant frequency using CSRR slot." IEEE Antennas and Wireless Propagation Letters (2023). https://doi.org/10.1109/LAWP.2023.3323008.

[15] Wang Xiang, and Xiao-Wei Zhu. "Compact and wideband filters based on slotline-perturbed quarter mode circular cavity substrate integrated waveguide." International Journal of RF and Microwave Computer-Aided Engineering 28, no. 9 (2018): e21542. https://doi.org/10.1002/mmce.21542.

[16] Chaturvedi Divya, Arvind Kumar, and S. Raghavan. "Compact QMSIW-based antenna with different resonant frequencies depending on loading of metalized vias." *International Journal of Microwave and Wireless Technologies* 11, no. 4 (2019): 420-427. https://doi.org/10.1017/S1759078719000126.

[17] Singh Jaget, F.Lohar, and B. S. Sohi. "Design of dual band millimeter wave antenna using SIW material for 5G cellular network applications." Materials Today: Proceedings 45 (2021): 5405-5409. https://doi.org/10.1016/j.matpr.2021.02.106.

[18] Chaturvedi Divya, Arvind Kumar, and Ayman A. Althuwayb. "A dual-band dual-polarized SIW cavity-backed antenna-duplexer for off-body communication." Alexandria Engineering Journal 64 (2023): 419-426. https://doi.org/10.1016/j.aej.2022.09.021.

[19] Niu Bing-Jian, and Jie-Hong Tan. "Compact self-isolated MIMO antenna system based on quarter-mode SIW cavity." Electronics Letters 55, no. 10 (2019): 574-576. https://doi.org/10.1049/el.2019.0606.

[20] Cui Jie, Feng-Xue Liu, Xiaopeng Shen, and et al. "Textile bandwidth-enhanced coupled-mode substrate-integrated cavity antenna with slot." Electronics 11, no. 15 (2022): 2454. https://doi.org/10.3390/electronics11152454.

[21] Altakhaineh Amjaad T., Saqer S. Alja'afreh, Aser M. Almatarneh, and et al. "A Quad-Band Shared-Aperture Antenna Based on Dual-Mode Composite Quarter-Mode SIW Cavity for 5G and 6G with MIMO Capability." *Electronics* 12, no. 11 (2023): 2480. https://doi.org/10.3390/electronics12112480.

[22] Memon Muhammad Usman, and Sungjoon Lim. "Review of reconfigurable substrate-integrated-waveguide antennas." *Journal of Electromagnetic Waves and Applications* 28, no. 15 (2014): 1815-1833. https://doi.org/10.1080/09205071.2014.960537.

[23] Moznebi Ali-Reza, Kambiz Afrooz, Mostafa Danaeian, and et al. "Four-way filtering power divider using SIW and eighth-mode SIW cavities with ultrawide out-of-band rejection." IEEE Microwave and Wireless Components Letters 29, no. 9 (2019): 586-588. https://doi.org/10.1109/LMWC.2019.2931115.

[24] Niu Bing-Jian, and Yan-Jie Cao. "Bandwidth-enhanced four-antenna MIMO system based on SIW cavity." *Electronics Letters* 56, no. 13 (2020): 643-645. https://doi.org/10.1049/el.2020.0799.

[25] Patel Pragati, and Yogesh Solunke. "New Wideband Vertical Tetraskelion-Shaped Dielectric Resonator Antenna." In *2020 IEEE 17th India Council International Conference (INDICON)*, pp. 1-6. IEEE, 2020. https://doi.org/10.1109/INDICON49873.2020.9342189.

[26] Sharma Indra Bhooshan, Fateh Lal Lohar, Prachi Joshi, and et al. "Multi-band antenna design by reshaping surface currents of higher order mode using CMA method." *IETE Journal of Research* 70, no. 6 (2024): 5572-5582. https://doi.org/10.1080/03772063.2023.2274908.

[27] Kumar Busineni Mahesh, Ayaz Ahmad, and Jayanta Mukherjee. "Wideband MIMO Antenna Based on Quarter-Mode SIW and 90-Degree Bent Planar Dipole." In *2021 IEEE International Symposium on Antennas and Propagation and USNC-URSI Radio Science Meeting (APS/URSI)*, pp. 1025-1026. IEEE, 2021. https://doi.org/10.1109/APS/URSI47566.2021.9704518.

[28] Niu Bingjian, and Jie-Hong Tan. "Compact four-element MIMO antenna system based on substrate-integrated-waveguide cavities." *Progress In Electromagnetics Research Letters* 88 (2020): 143-149. http://dx.doi.org/10.2528/PIERL19102701.

[29] Onay, Muhammed Yusuf, and Burak Dokmetas. "3D Printed microstrip antenna for symbiotic communication: WiFi backscatter and bit rate evaluation for IoT." Internet of Things (2025): 101643. https://doi.org/10.1016/j.iot.2025.101643.

[30] Dokmetas Burak, Galip Orkun Arican, and Burak Alptug Yilmaz. "A Folded Pyramid-Shaped Microstrip Antenna with Improved Bandwidth." In *2024 IEEE International Symposium on Antennas and Propagation and INC/USNC-URSI Radio Science Meeting (AP-S/INC-USNC-URSI)*, pp. 1273-1274. IEEE, 2024. https://doi.org/10.1109/AP-S/INC-USNC-URSI52054.2024.10686622.

Figures Captions List

Figure1. Schematic of Antenna, (a) Single EMSIW antenna, (b) 2*2 MIMO antenna.
Figure 2. Modal analysis of square SIW resonator, (a) FMSIW Resonator, (b) HMSIW Resonator, (c) QMSIW Resonator, and (d) EMSIW resonator.
Figure 3. the E-field distributions of Square SIW resonator up to 4 modes (a) at fundamental mode 2.5 GHz, (b & c) higher orthogonal modes at 4.5 GHz, and (d) higher mode at 5.8 GHz

Table Captions List

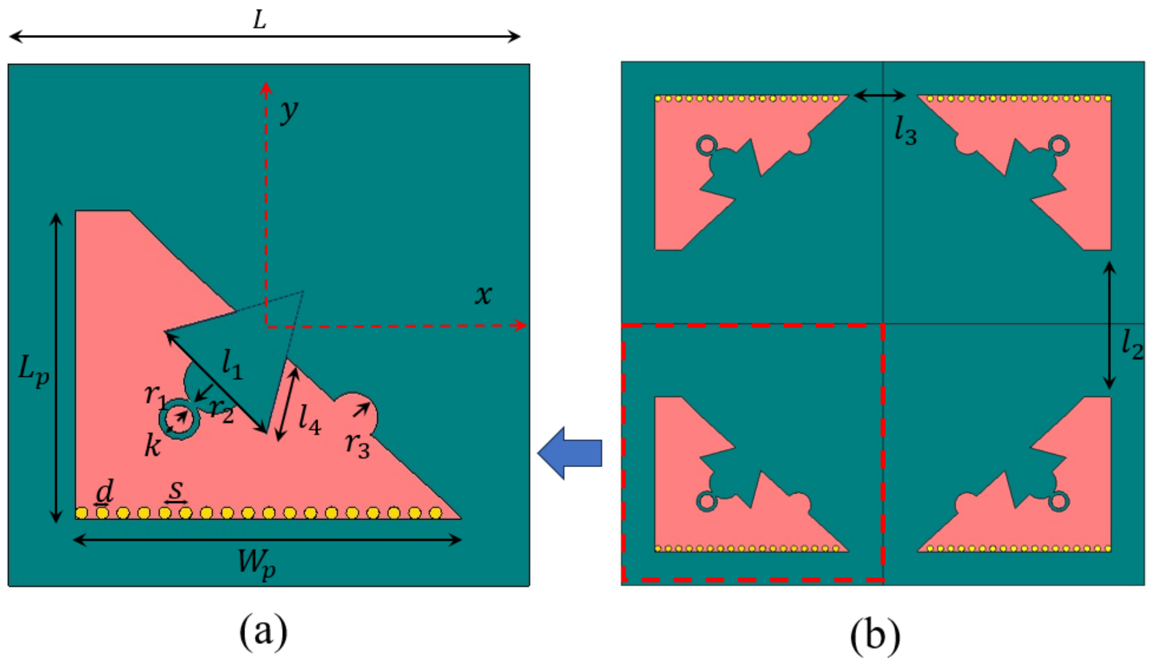

Figure 1. Schematic of Antenna, (a) Single EMSIW antenna, (b) 2*2 MIMO antenna.

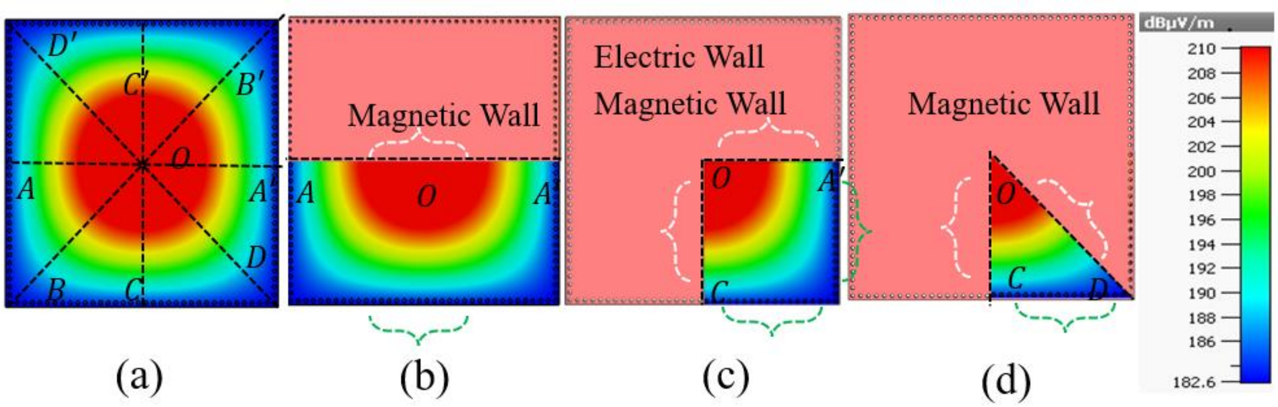

Figure.2 Modal analysis of square SIW resonator, (a) FMSIW Resonator, (b) HMSIW Resonator, (c) QMSIW Resonator, and (d) EMSIW resonator.

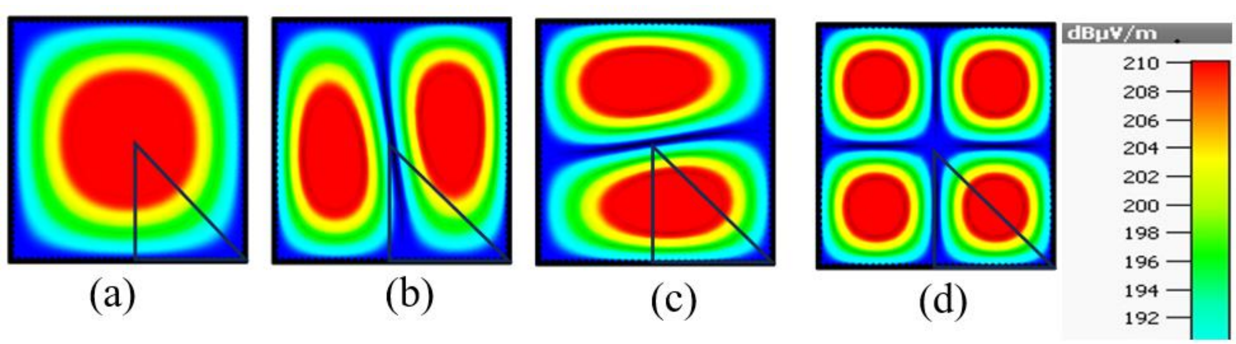

Figure3. the E-field distributions of Square SIW resonator up to 4 modes (a) at fundamental mode 2.5 GHz, (b & c) higher orthogonal modes at 4.5 GHz, and (d) higher mode at 5.8 GHz

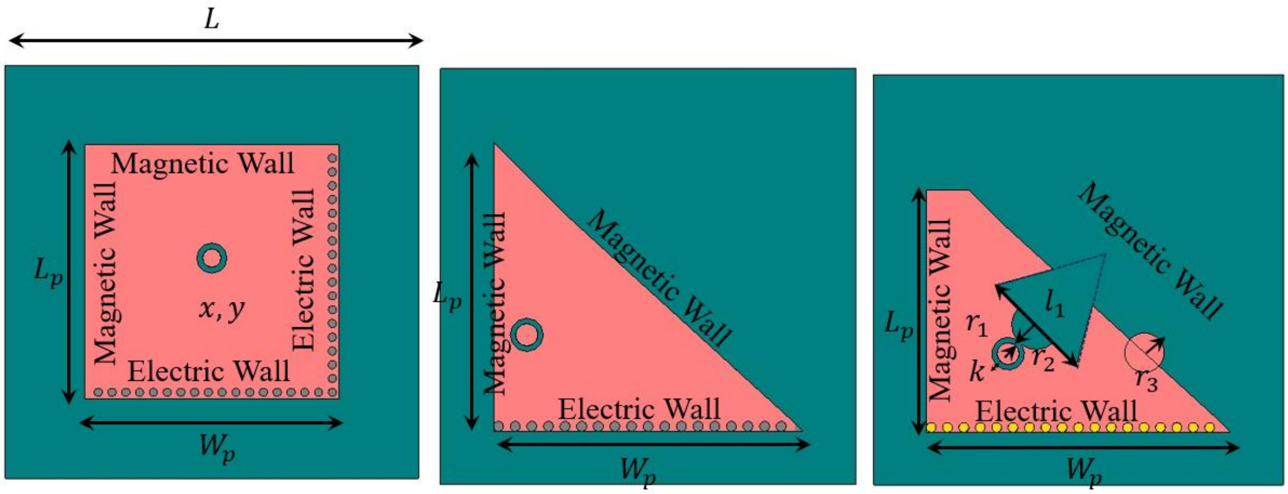

(a) (b) (c)

Figure4 Designing SIW Antenna, (a) conventional QMSIW Antenna, (b) EMSIW Slot loaded EMSIW Antenna.

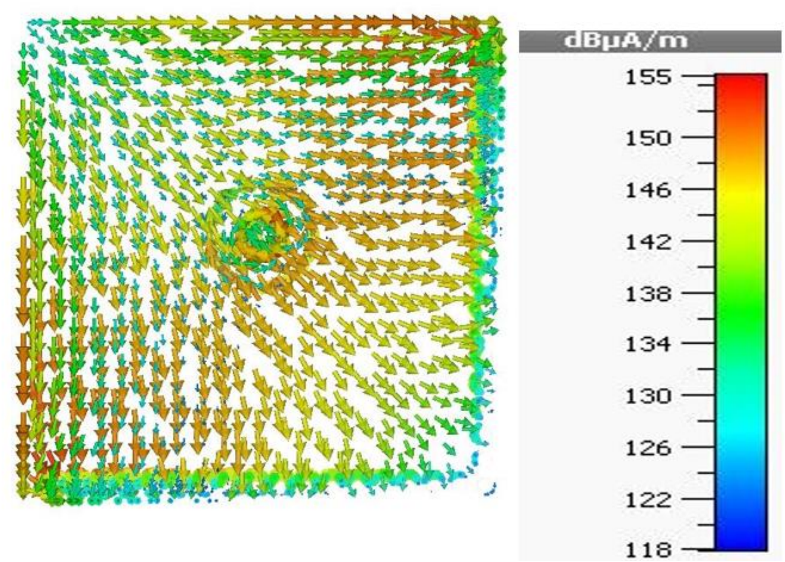

(a)

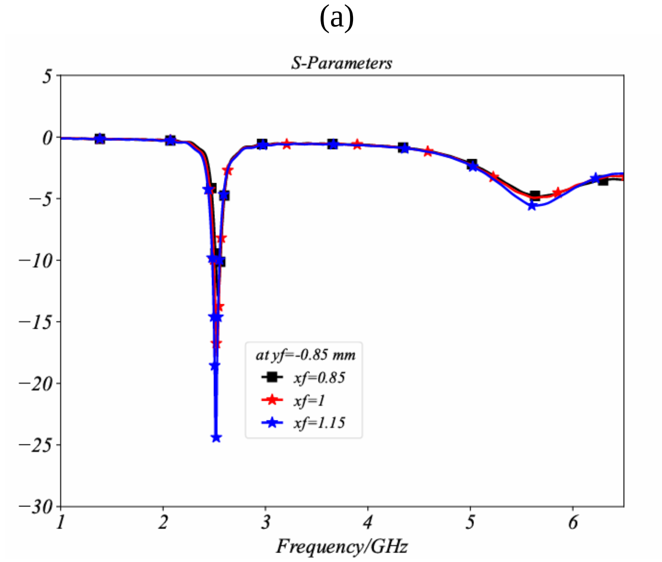

(b)

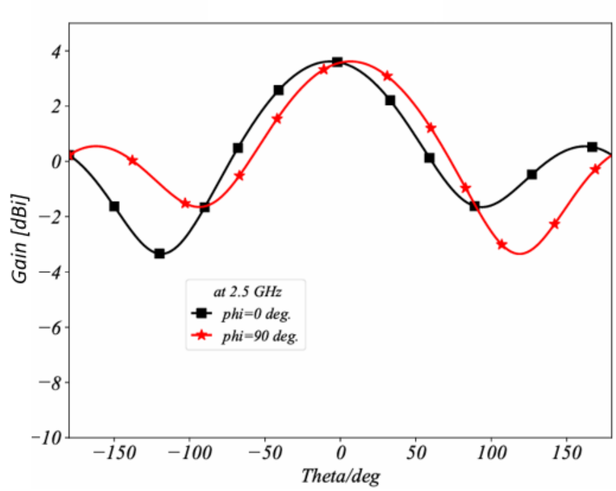

(c)

Figure5 (a) shows the surface current distribution of a conventional QMSIW antenna operating at 2.5 GHz.

Figure5 (b) S11 plot for parametric feed location study of conventional QMSIW Antenna.

Figure5 (c) Far-Field Radiation pattern of conventional QMSIW Antenna.

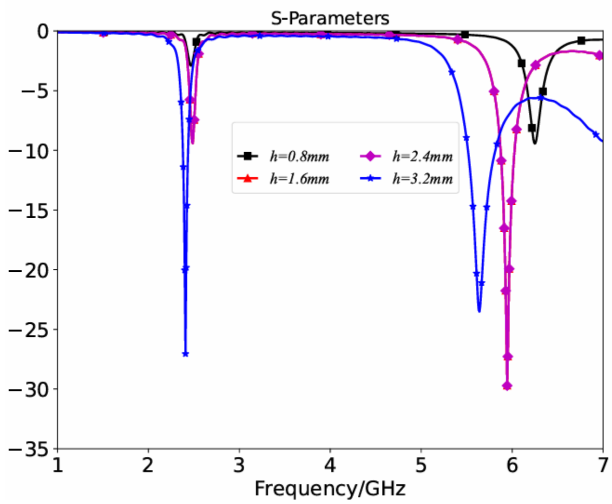

(a)

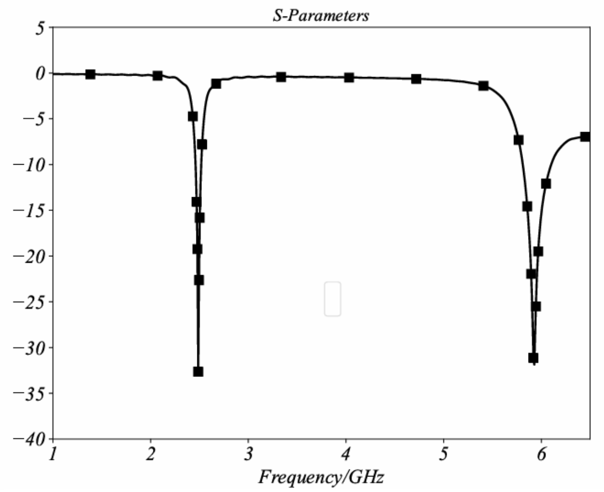

(b)

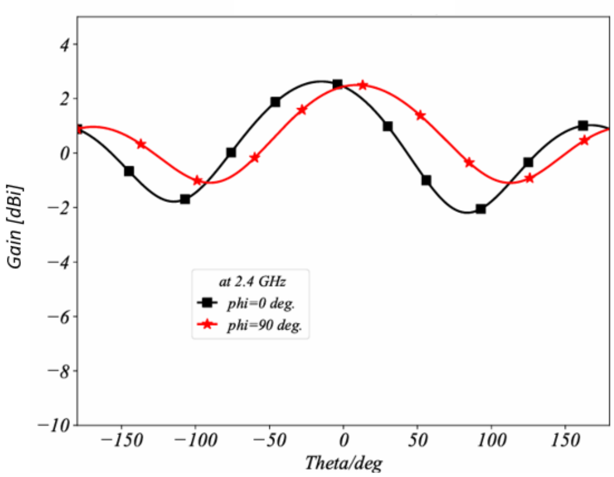

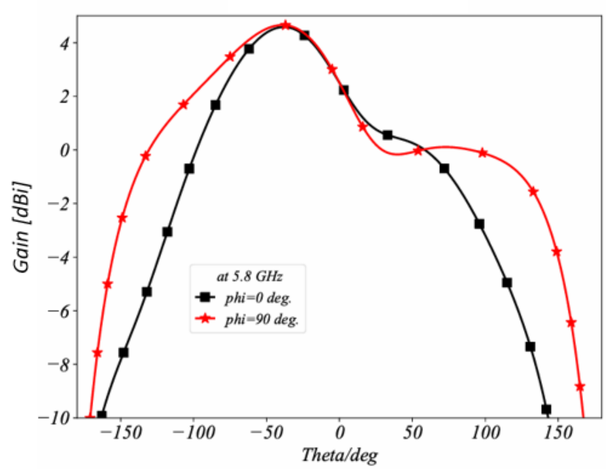

(c) (d)

Figure6 (a) Parametric study illustrating the effect of substrate height (h) on the bandwidth performance.
Figure6 (b) S11 plot of dual band EMSIW Antenna.
Figure6(c) Far-Field Radiation pattern of EMSIW Antenna at 2.5GHz.
Figure6(d) EMSIW Antenna Far-Field Radiation Pattern at 5.8GHz.

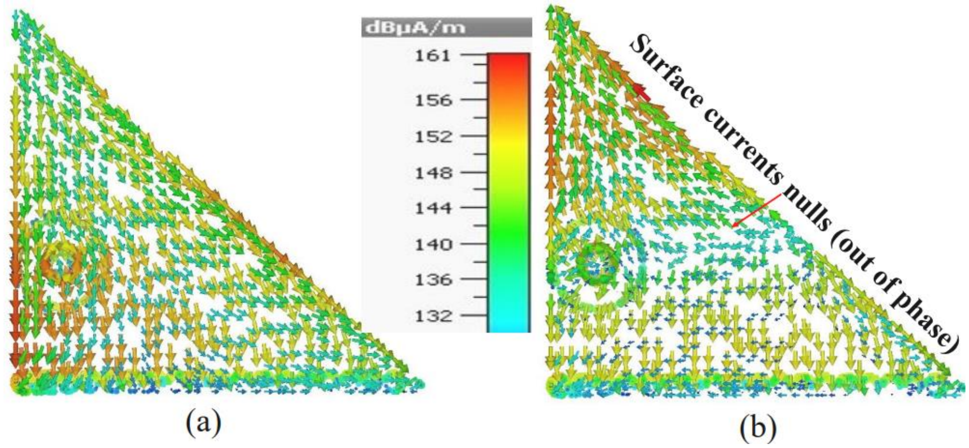

Figure7 shows the surface current distribution at 2.5 GHz and 5.8 GHz of the conventional EMSIW antenna.

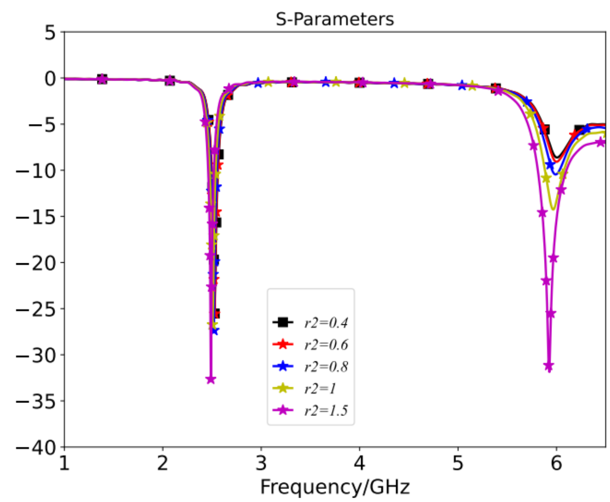

(a)

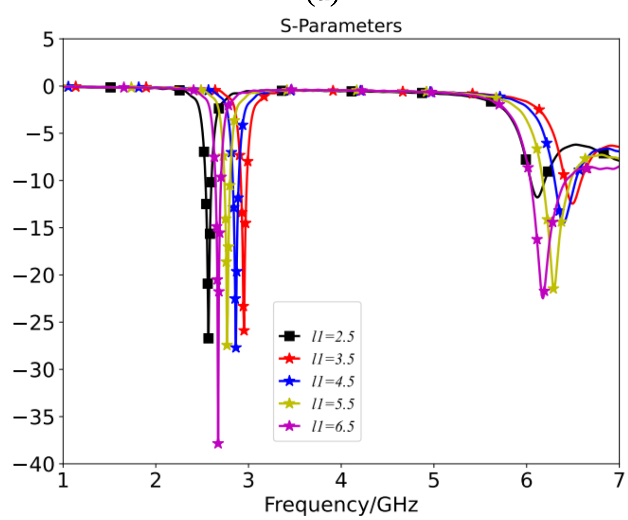

(b)

Figure8(a) S11 plot for parametric r2 study of Slotted EMSIW Antenna.
Figure8 (b) S11 plot for parametric l2 study of Slotted EMSIW Antenna.

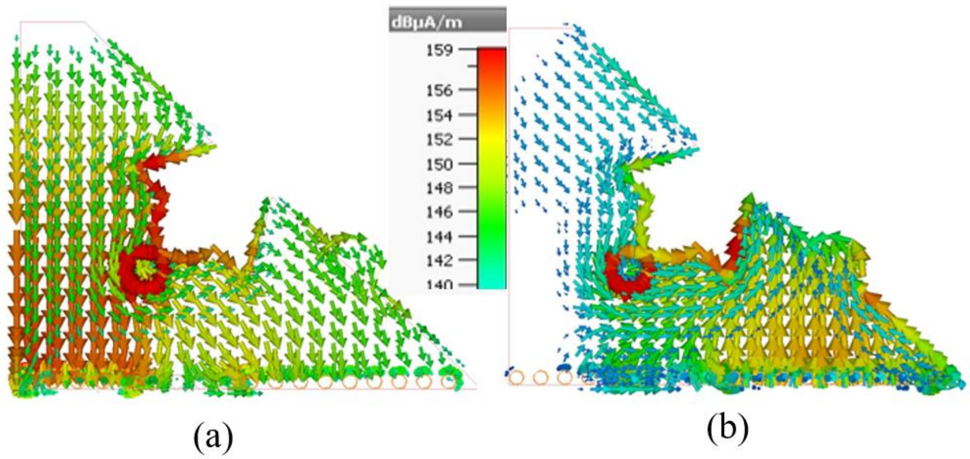

Figure9. Surface Current Distribution of Slotted EMSIW Antenna, (a) at 2.5 GHz and (b) 5.8GHz.

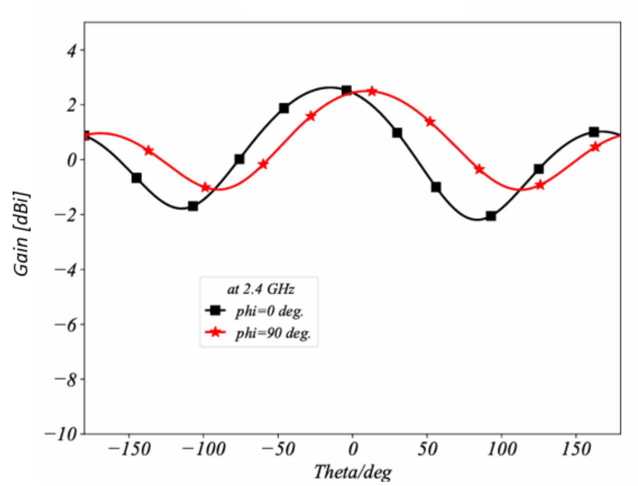

(a)

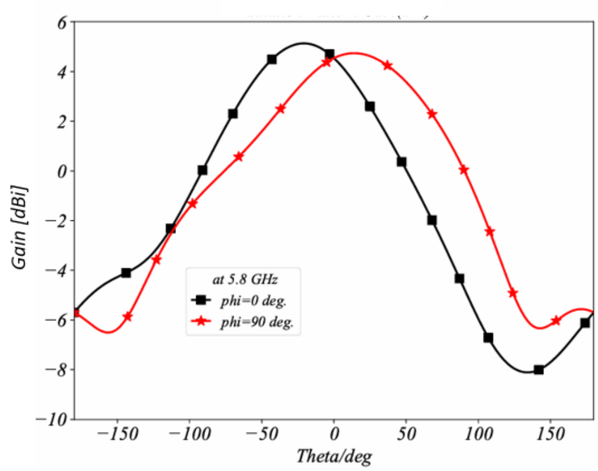

(b)

Figure 10(a) Far-Field Radiation pattern of slotted EMSIW Antenna at 2.4 GHz.
Figure 10(b) Far-Field Radiation pattern of slotted EMSIW Antenna at 5.8 GHz.

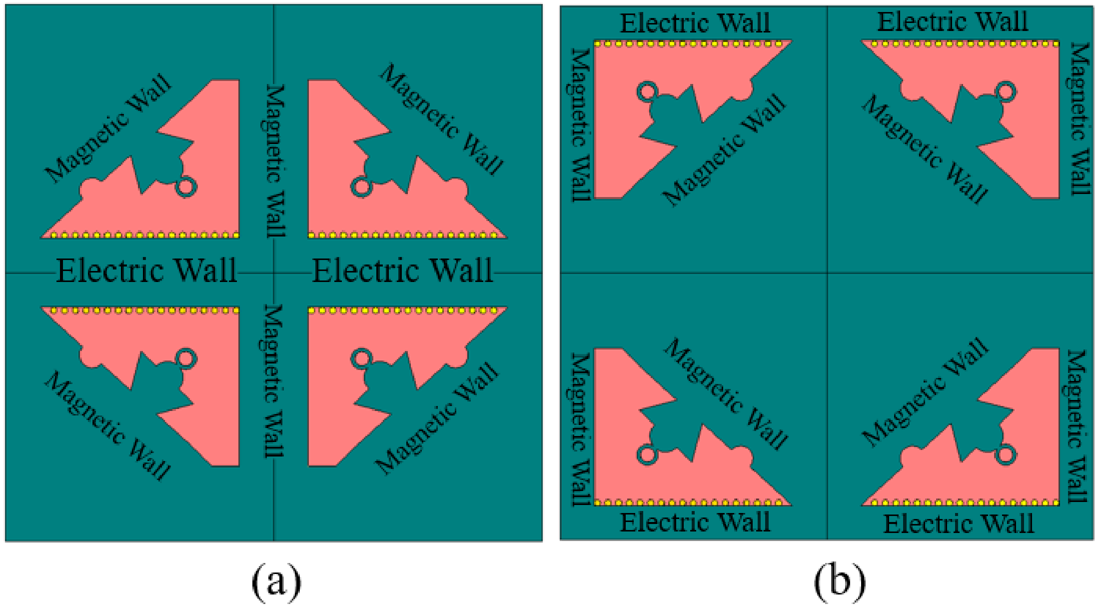

Figure 11. 2×2 MIMO antenna element arrangements for mutual coupling performance study. (a) case-1. (b) case-2.

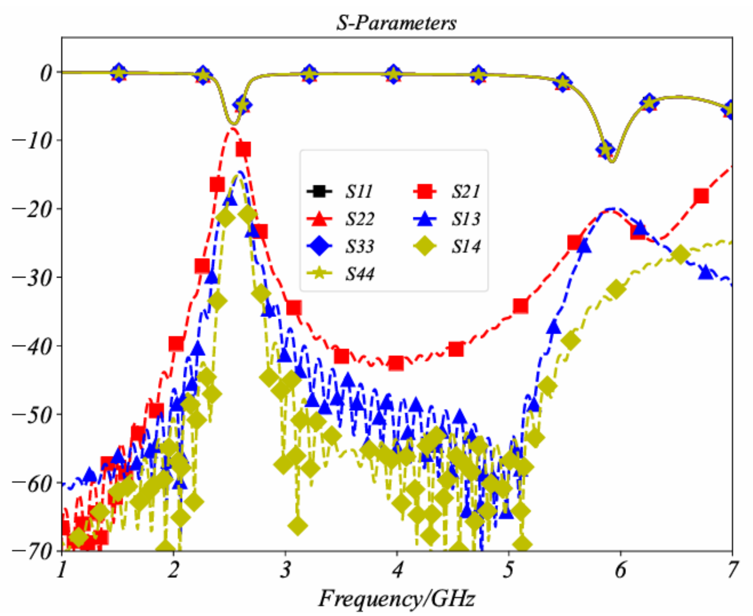

Figure 12. Scattering Parameters for case-1 EMSIW MIMO antenna.

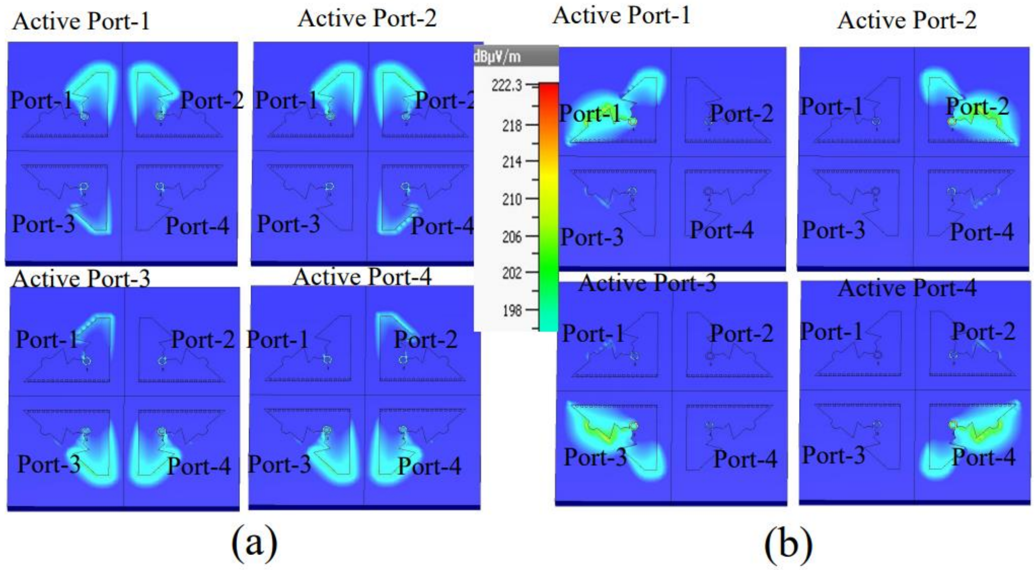

Figure 13. surface current for case-1 EMSIW MIMO antenna, (a) at 2.5 GHz, (b) at 5.8 GHz.

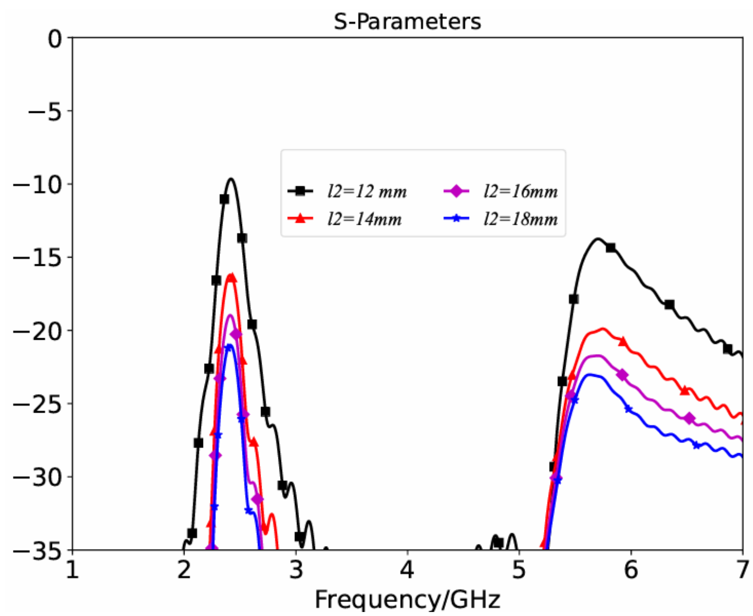

Figure 14. Parametric study of the mutual coupling parameter l2 for the EMSIW MIMO antenna.

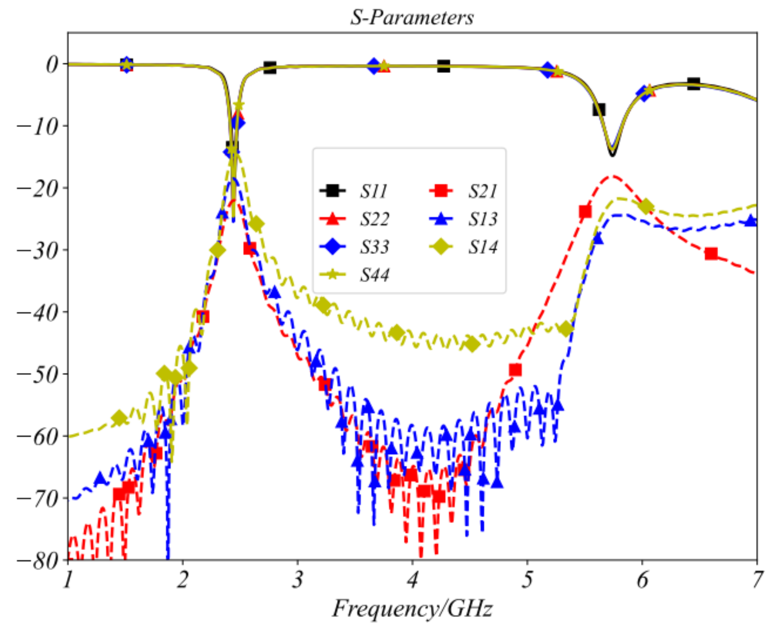

Figure 15. Scattering Parameters for case-2 EMSIW MIMO antenna.

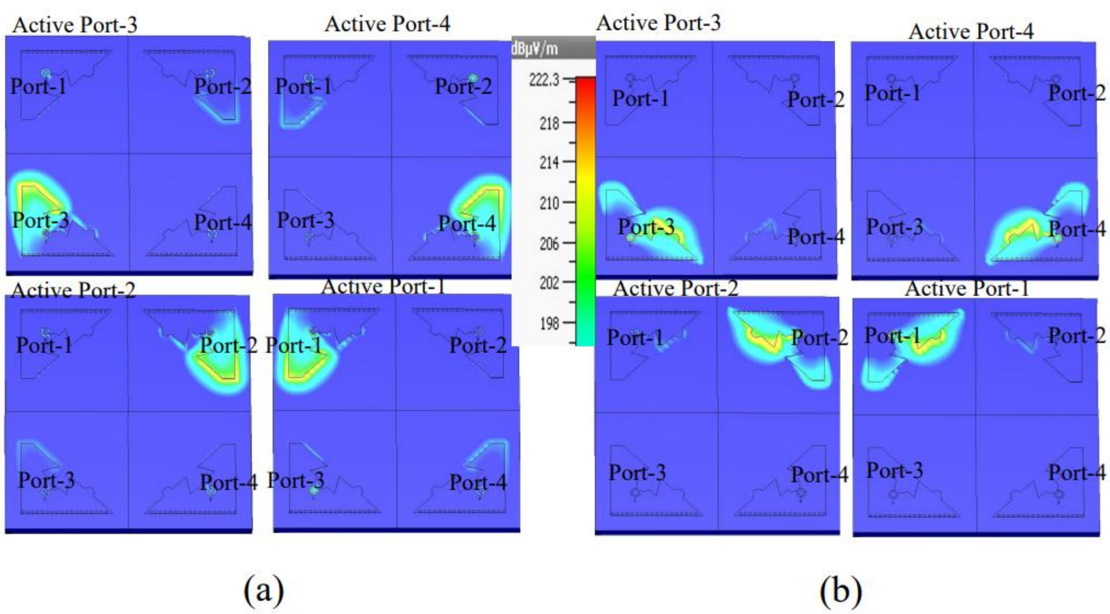

Figure 16. surface current for case-2 EMSIW MIMO antenna, (a) at 2.5 GHz, (b) at 5.8 GHz.

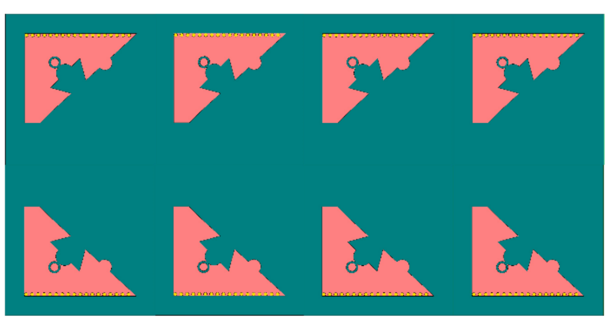

(a)

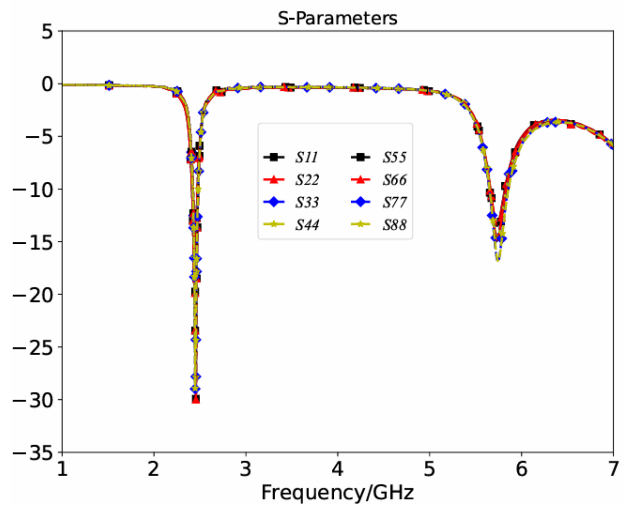

(b)

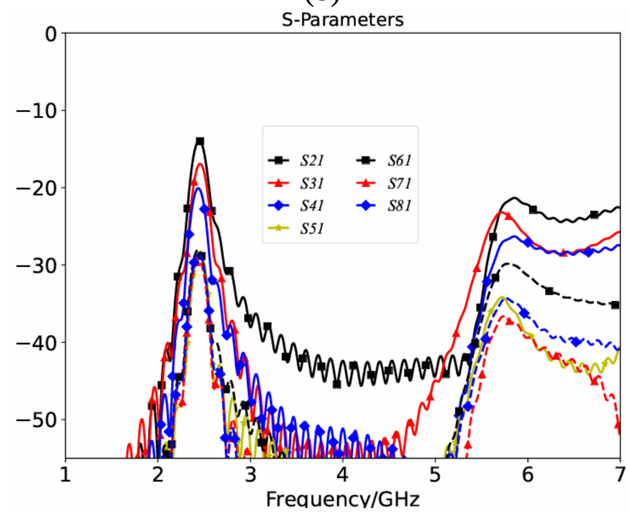

(c)

Figure 17(a) 4×4 MIMO antenna element arrangements.
Figure17 (b) S11-parameters of 4×4 MIMO antenna.
Figure 17(c) S21-parameters of 4×4 MIMO antenna.

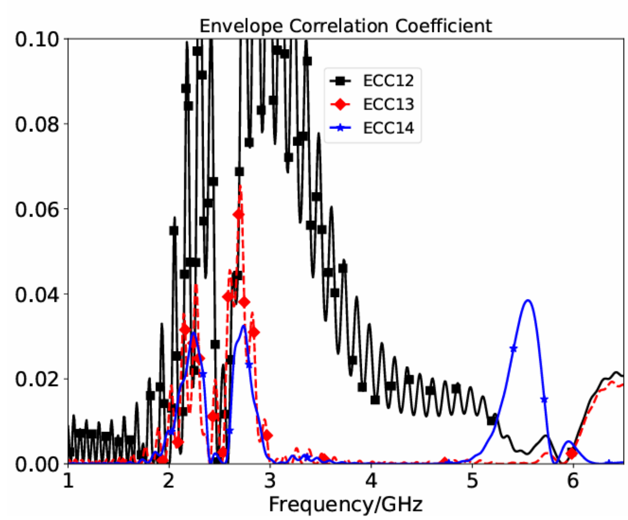

(a)

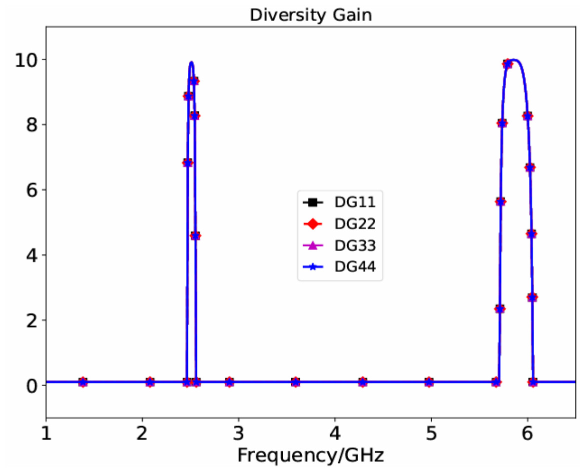

(b)

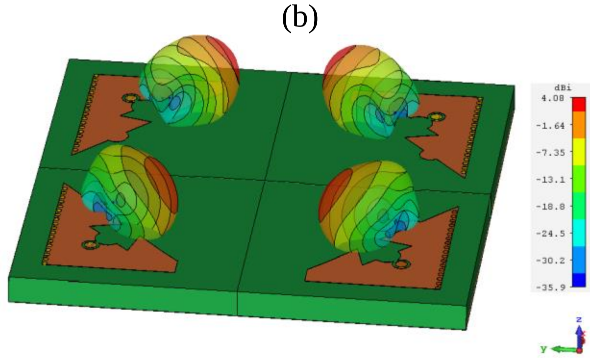

(c)

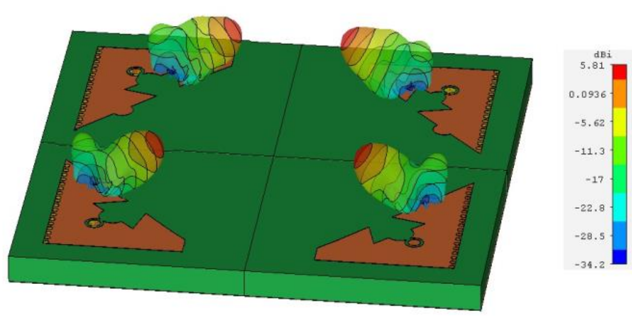

(d)

Figure 18(a) Simualted ECC of 2*2 MIMO antenna.
Figure 18(b) Simualted Diversity gain of 2*2 MIMO antenna.
Figure 18(c) Far field radition pattern 2*2 MIMO antenna at 2.5 GHz.
Figure 18(d) Far field radition pattern 2*2 MIMO antenna at 5.8 GHz.

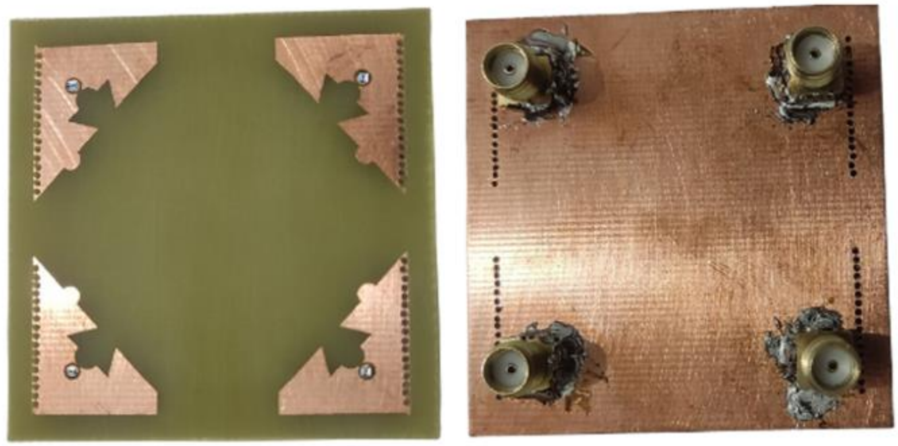

(a) (b)

Figure 19. illustrate 2*2 MIMO antenna, (a) front view, (b) back view.

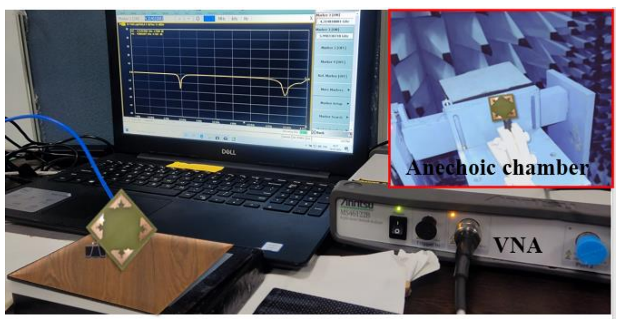

(a)

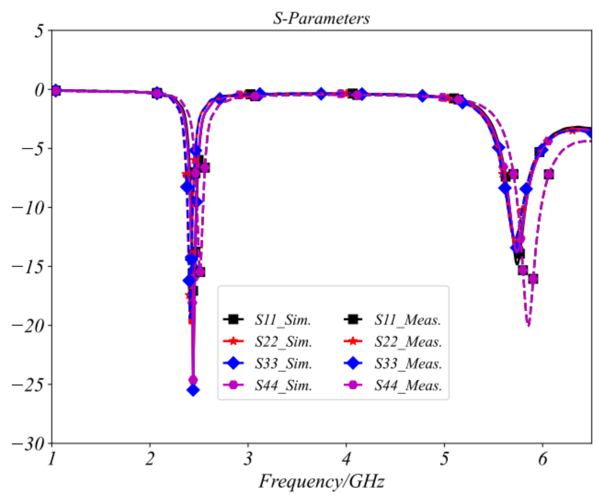

(b)

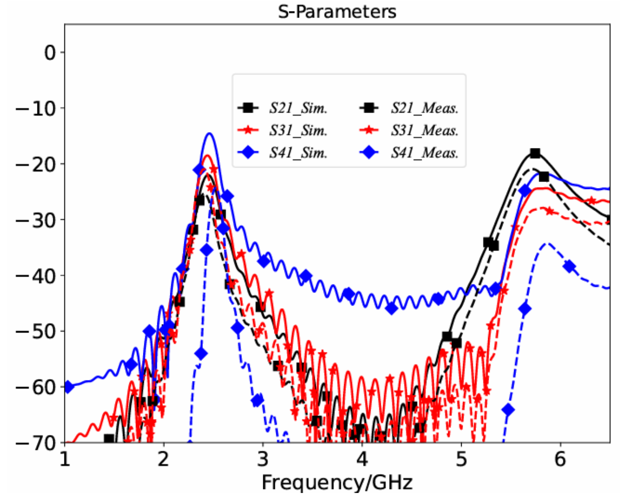

(c)

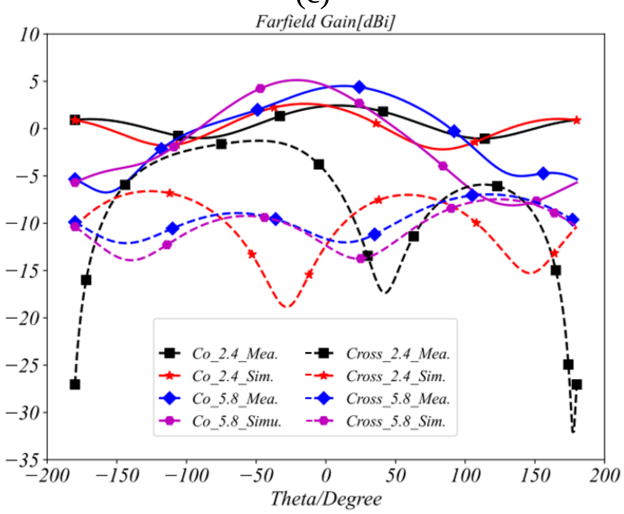

(d)

Figure 20(a) illustrate 2*2 MIMO antenna measurement set -up.
Figure 20(b) Shows the comparison S11 parameters between simulation and measurement.
Figure 20(c) Shows the comparison S21 parameters between simulation and measurement.
Figure 20(d) Shows the comparison farfield gain patterns at 2.4 and 5.8 GHz frequency.

TABLE I
PROPOSED ANTENNA PARAMETERS

Parameters	Values(mm)	Parameters	Values(mm)
L	25	r_3	1.50
L_p	15.80	l_1	6.50
W_p	18.55	l_2	14
l_4	3.76	l_3	6.50
k	0.33	d	0.6
r_1	0.67	s	1
r_2	1.50	h	2.4

TABLE II
RELATIVE WORK COMPARISON TABLE WITH PROPOSED

Ref.	Size (λ_o)	Frequency Bands (GHz)	Methods	Gain (dBi)	Port Isolation	ECC
[4]	0.84*0.48	3.7-4.3	coupling slot	2	>22	-
[5]	0.69*0.52	5.2	line de-coupling	2	>22	-
[6]	0.70*0.44	3.3-7.8	Decoupling Structure	3.2	>20	<0.06
[8]	1.11*1.11	3.1-11.11	Parasitic de-Coupler	3.4	20	0.001
[9]	1.29*0.64	1.92-2.51	Decoupling element	3.8	>15	0.0037
[10]	0.28*0.28	2.42-7.45	Stub Loading	2.5	>12	0.004
[11]	0.45*0.15	3.3-3.6, 4.4-5	Orthogonal Modes	3.6	>24	0.008
[21]	0.09*0.43	3.4-3.6, 4.8-5	Stop filter	4	>12	-
[24]	0.23*0.06	3.37-3.61,4.9-5.1	-	3	>14	0.06
This Work	**0.41*0.41**	**2.5, 5.8**	**SIW with Electric Wall**	**2.6, 5.2**	**>25.5**	**0.001**

Nidhi Yadav received a B.E. degree in Electronics and Communication Engineering from the Birla Institute of Technology, Mesra, India, in 2014 and an M.Tech. degree in Electronics and Communication Engineering from Malviya National Institute of Technology, Jaipur, India, in 2017. She is currently working toward her PhD degree at MNIT Jaipur since 2021. She is presently working as a Lecturer at Government Polytechnic College, Board of Technical Education Rajasthan. Her main areas of interest are microstrip, reconfigurable and MIMO antennas.

Rajendra P. Yadav is currently working as a professor with the Department of Electronics and Communication Engineering, Malaviya National Institute of Technology, Jaipur, India. Besides being an able academician and administrator (Ex Vice Chancellor of Rajasthan Technical University, Kota and Ex Chairman NWRC Chandigarh AICTE), Rajendra is actively engaged in research in communication engineering, MEMS, MIMO-OFDM, multi user detection, microstrip antenna and arrays, optical communication, and engineering education.

Mahendra Mohan Sharma received a B.E. degree in 1985 from NIT, Srinagar, India. He did an M.Tech. from IIT, Delhi, and PhD from MNIT, Jaipur, India. He joined as a Lecturer in the Department of Electrical Engineering, MNIT, Jaipur, in 1986 and was designated as an Associate Professor there in 1995. Presently, He is working as a Professor with the Department of Electronics and Communication Engineering, MNIT Jaipur. Besides being an able academician and administrator (Registrar in MNIT and Ex Executive Director at National Institute of Electronics and Information Technology, Chandigarh). He is an active member of IEEE, Broadcasting Engineering Society (India), and a Life Senior Member of ISTE professional bodies. He is the Honorary Secretary of the IEEE-MTTS India Council Chapter. He is the author/coauthor of more than 100 research papers published in international/national journals and conferences. His research interests include the design and modelling of antennas, arrays, and FSS.